Journal of
Synchrotron
Radiation

ISSN 0909-0495

Received 29 April 2011
Accepted 11 August 2011

The status of strontium in biological apatites: an XANES investigation

D. Bazin,[a]* M. Daudon,[b] Ch. Chappard,[c] J. J. Rehr,[d] D. Thiaudière[e] and S. Reguer[e]

[a]Laboratoire de Physique des Solides, Bâtiment 510, Université Paris XI, 91405 Orsay, France, [b]Laboratoire de Biochimie A, Hôpital Necker-Enfants Malades, AP-HP, 149 Rue de Sèvres, 75743 Paris Cedex 15, France, [c]B2OA, UMR 7052 CNRS, Université Paris Diderot, 10 avenue de Verdun, 75010 Paris, France, [d]Department of Physics, University of Washington, Seattle, WA 98195, USA, and [e]Synchrotron SOLEIL, L'Orme des Merisiers, Saint-Aubin, BP 48, 91192 Gif-sur-Yvette, France. E-mail: bazin@lps.u-psud.fr

Osteoporosis represents a major public health problem and increases patient morbidity through its association with fragility fractures. Among the different treatments proposed, strontium-based drugs have been shown to increase bone mass in postmenopausal osteoporosis patients and to reduce fracture risk. While the localization of Sr^{2+} cations in the bone matrix has been extensively studied, little is known regarding the status of Sr^{2+} cations in natural biological apatite. In this investigation the local environment of Sr^{2+} cations has been investigated through XANES (X-ray absorption near-edge structure) spectroscopy in a set of pathological and physiological apatites. To assess the localization of Sr^{2+} cations in these biological apatites, numerical simulations using the *ab initio FEFF9* X-ray spectroscopy program have been performed. The complete set of data show that the XANES part of the absorption spectra may be used as a fingerprint to determine the localization of Sr^{2+} cations *versus* the mineral part of calcifications. More precisely, it appears that a relationship exists between some features present in the XANES part and a Sr^{2+}/Ca^{2+} substitution process in site (I) of crystal apatite. Regarding the data, further experiments are needed to confirm a possible link between the relationship between the preparation mode of the calcification (cellular activity for physiological calcification and precipitation for the pathological one) and the adsorption mode of Sr^{2+} cations (simple adsorption or insertion). Is it possible to draw a line between life and chemistry through the localization of Sr in apatite? The question is open for discussion. A better structural description of these physiological and pathological calcifications will help to develop specific therapies targeting the demineralization process in the case of osteoporosis.

Keywords: Ca phosphate apatites; physiological calcifications; pathological calcifications; Fourier transform infrared spectroscopy X-ray absorption spectroscopy; strontium environment.

1. Introduction

Osteoporosis represents a major public health problem and increases patient morbidity through its association with fragility fractures. Fractures of the hip and vertebrae especially imply significant mortality. From an epidemiologic point of view, about ten million Americans older than 50 have osteoporosis, and a further 34 million are at risk of the disease (Cooper, 1999; Holroyd *et al.*, 2008). Among the different treatments proposed, strontium-based drugs such as strontium ranelate (PROTELOS), which combines two strontium cations and an organic carrier, ranelic acid, have shown anti-fracture efficacy in the treatment of postmenopausal osteoporosis (Meunier *et al.*, 2004). Such treatments have been shown also to increase bone mass in postmenopausal osteoporosis patients (Boivin *et al.*, 1996; Farlay *et al.*, 2005; Marie, 2005; Roux, 2007; Rochefort *et al.*, 2010; Roschger *et al.*, 2010). Many studies have been performed to investigate the spatial repartition in tissues as well as the local environment of this oligoelement (Dahl *et al.*, 2001; Verberckmoes *et al.*, 2004; Korbas *et al.*, 2004; Zhang *et al.*, 2005; Ni *et al.*, 2006; Bradley *et al.*, 2007*a*,*b*; Zoeger *et al.*, 2008; Zheng *et al.*, 2009; Bellis *et al.*, 2009).

Regarding Sr^{2+} cation localization in bone, different structural hypotheses taking into account the physicochemistry of biological apatite can be elaborated. First, Sr^{2+} cations are

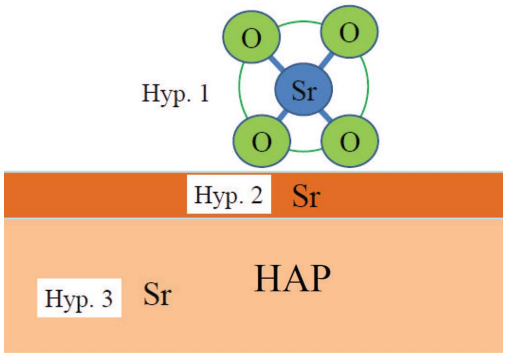

Figure 1
Schematic representation of the three structural hypotheses assessed in this study regarding the localization of Sr^{2+} cations in HAP (hydroxyapatite).

adsorbed at the surface of collagen or apatite surrounded only by O atoms (hypothesis 1 in Fig. 1). Secondly, Sr^{2+} cations could be engaged in the hydrated poorly crystalline apatite region present at the surface of calcium phosphate nanocrystals (hypothesis 2 in Fig. 1). Finally, a substitution could occur between Sr^{2+} cations and Ca^{2+} cations inside calcium phosphate nanocrystals on either crystallographic site (I) or (II) (hypothesis 3 in Fig. 1).

Sr is also present in apatites involved in pathological calcifications. For such biological samples the key point comes from the fact that oligoelements may control the nanocrystalline morphology which constitutes the calcification (Oka *et al.*, 1987; Grases *et al.*, 1989). It is worth mentioning that nanocrystal morphology is a key parameter for medical diagnosis (Daudon *et al.*, 1993). In the case of kidney stones, depending on the morphology, the associated pathology has either a dietary or a severe genetic origin (Daudon *et al.*, 2008, 2009). Regarding bones, a recent investigation (Li *et al.*, 2010) has shown, through X-ray scattering, that strontium is incorporated into crystalline minerals only in newly formed bone during strontium ranelate treatment. As underlined in several publications, scattering techniques (Guinier, 1956; Fratzl *et al.*, 1996; Camacho *et al.*, 1999) are sensitive to strontium content within the mineral crystals, but ignore other types of non-crystalline strontium deposits.

The present study was designed to investigate the local environment of Sr^{2+} cations through X-ray absorption spectroscopy (XAS) in a set of biological apatites engaged in physiological as well as pathological calcifications. XAS (Sayers *et al.*, 1971) is especially useful for characterizing such calcifications (Binsted *et al.*, 1982; Hukins *et al.*, 1986; Harries *et al.*, 1987; Peters *et al.*, 2000; Bazin *et al.*, 2009*a*,*b*; Nguyen *et al.*, 2011). As underlined previously, scattering techniques are sensitive only to strontium content within the mineral crystals and biological compounds may be poorly crystalline or amorphous. XAS yields an average structural description of the local environment of Sr^{2+}, this average being made over all Sr^{2+} present in the sample, including crystalline and non-crystalline strontium entities. Even if XAS is insensitive to polydispersity (Moonen *et al.*, 1995), XAS constitutes an elegant complementary structural description to structural data obtained from scattering techniques for materials without long-range order (Bazin *et al.*, 1997*a*). In addition, measurements can be performed directly on a sample with minimal preparation.

As emphasized previously (Bazin *et al.*, 2006), XAS encompasses both XANES and extended X-ray absorption fine structure (EXAFS), and provides an opportunity to evaluate the local order around each element selected through its absorption edge. The present study is based on the XANES part of XAS to evaluate the local environment of Sr^{2+} cations on a set of physiological and pathological calcifications. Moreover, a set of numerical simulations using the *FEFF9* program (Rehr *et al.*, 2009; Ankudinov *et al.*, 1998, 2002) have been performed in order to assess the localization of Sr^{2+} cations inside the apatite crystal.

Table 1
Composition given by FTIR and the origin of the calcifications.

CA = carbonated calcium hydroxylapatite. ACCP = amorphous carbonated calcium phosphate. Prot = Protein. C1 = whewellite. C2 = weddellite. TRG = triglyceride.

Sample	Origin of the calcification	Composition as given by FTIR
N 11823	Kidney	66% CA, 30% ACCP, 4% Prot
N 13066	Kidney	79% CA, 15% ACCP, 4% Prot, 2% C1
N 13086	Prostate	84% CA, 12% Prot, 4% C1
N 15048	Kidney	87% CA, 6% C1, 4% C2, 3% Prot
N 17161	Bladder	61% CA, 30% ACCP, 8% Prot, 1% C1
Ag Cart	Bone	70% CA, 20% Prot, 10% TRG
Bp Cart	Bone	75% CA, 20% Prot, 5% TRG
VE Cart	Bone	70% CA, 15% Prot, 15% TRG
VM Cart	Bone	80% CA, 15% Prot, 5% TRG

2. Materials and methods

The biological samples (Table 1) analysed in the present investigation came from two different institutions. More precisely, kidney stones and bones came from Necker Hospital and Lariboisière Hospital (Paris), respectively.

All the samples have been characterized by Fourier transform infrared (FTIR) spectroscopy (Paschalis *et al.*, 2011). To do so, an FTIR spectrometer, Vector 22 (Bruker Spectrospin, Wissembourg, France), was used according to the analytical procedure previously described (Estepa & Daudon, 1997). Data were collected in the absorption mode between 4000 and 400 cm^{-1} with a resolution of 4 cm^{-1}.

All the samples were investigated on the DIFFABS beamline at synchrotron SOLEIL (France). This experimental set-up is mainly dedicated to structural characterization by combining, when necessary, X-ray diffraction, X-ray absorption and X-ray fluorescence spectroscopies. The SOLEIL synchrotron was running at 2.75 GeV with an average current of 300 mA in the new TOP/UP mode. Details regarding the monochromator, the mirror, as well as the devices used for the detection on DIFFABS, are described in previous studies (Bazin *et al.*, 2008; Carpentier *et al.*, 2010). In the present case, the beamline was optimized in order to measure XANES at the Sr *K*-edge. The energy range was selected between 16000

and 16200 eV, with an energy step of 0.5 eV and a 3 s acquisition time. The size of the beam was determined by a set of slits (100–500 µm).

The *ab initio FEFF9* code (Rehr *et al.*, 2000, 2009) is quite useful for performing full multiple-scattering calculations in real space for crystalline as well as for nanometer scale solids, either at the *K*- or *L*-edges (Bazin *et al.*, 1997*b*; Bazin & Rehr, 2003). Structural as well as electronic information is contained in the modulations superimposed on the otherwise smooth atomic absorption coefficient. In the EXAFS module of *FEFF9*, the oscillatory structure is expressed as a sum of independent multiple-scattering contributions. Each contribution can be expressed in the following form,

$$\chi^n(k) = \chi_0^n(k)\exp\left(-L_n/\lambda_n - 2k^2\sigma_n^2\right), \quad (1)$$

$$\chi_0^n(k) = F_n(k)\sin\left[kL_n + \theta_n(k)\right], \quad (2)$$

where we have separated the oscillatory and damping terms from the mean free path and disorder. As previously described, n represents different single- or multiple-scattering paths and L_n is the total path length; F and θ_n are the amplitude and phase which depend on the photoelectron wavenumber k, on the specifics of the scattering path n, and on the atomic potential parameters. For XANES spectra, these multiple-scattering path contributions can also be summed to all orders by matrix inversion methods, as implemented in the full multiple-scattering algorithms in *FEFF9*.

3. Results

XANES spectra collected at the Sr *K*-edge, for physiological (bones) as well as pathological (kidney stones) calcifications, are plotted in Fig. 2. Beyond an intense white line, which reflects the effective charge of Sr^{2+} ions ($4d^0$ electron configuration), only one oscillation (16163 eV) is measured in the case of kidney stones (Fig. 2), while for bones a small feature exists (at 16135 eV) just after the white line and before the first oscillation.

In order to extract significant structural information from such XANES spectra, a set of numerical simulations using the *FEFF9* program have been performed. Hydroxyapatite (HAP) can be described as a hexagonal stacking of $(PO_4)^{3-}$ groups with two kinds of tunnels parallel to the *c*-axis (Elliott, 1994; Brown & Constantz, 1994; Wilson & Elliott, 1999; White & ZhiLi, 2003). The first coincides with the ternary axis of the structure and is occupied by Ca^{2+}, noted as Ca^{2+}(I) ions. The second is linked by oxygen and other calcium ions, noted Ca^{2+}(II), and is occupied by OH^- ions. Ca^{2+}(I) and Ca^{2+}(II) are present in a 2:3 ratio.

Regarding the replacement of Ca^{2+} cations by other cations, numerous studies have been performed in order to locate the foreign cations in the HAP structure. Occupation depends on the dimension of the cations (Tamm & Peld, 2006). Larger ones are preferentially occupied by the Ca^{2+}(II) sites, since in site Ca^{2+}(II) the arrangement of the staggered equilateral triangles allows the optimization of the packing of large ions. In the opposite way, for the Ca^{2+}(I) crystallographic site, the strict alignment in the columns causes a stronger repulsion. Some authors have recently noted that Zn atoms may occupy interstitial sites in HAP (Gomes *et al.*, 2011).

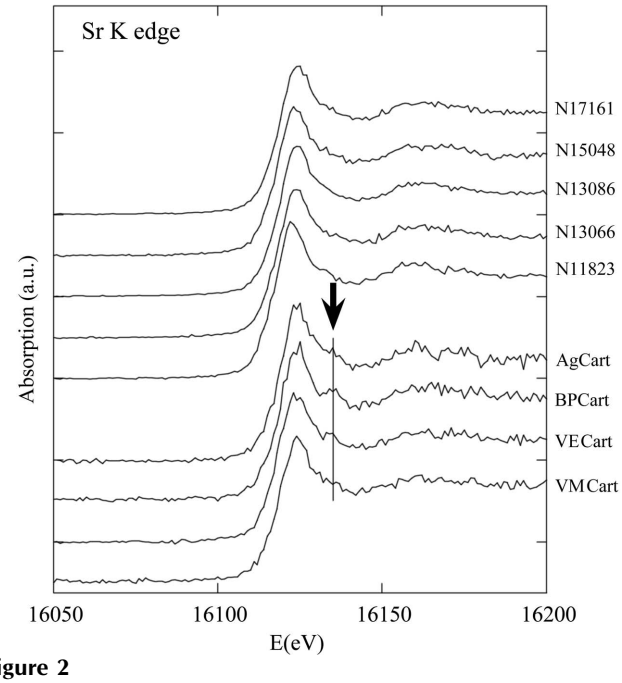

Figure 2
XANES spectra recorded at the Sr *K*-edge (E = 16109 eV) for different pathological calcifications (kidney stones) and a set of physiological calcifications (bones).

We have performed a set of numerical simulations taking into account the location of Sr^{2+} cations either in crystallographic site (I) or in site (II). For each crystallographic site we performed several simulations in order to assess the different structural hypotheses previously selected. For example, for the simulation labelled Sr^{2+}(I)-O, the local environment of Sr^{2+} cations is made only by O atoms (details regarding the spatial repartition of O atoms around Sr^{2+} cations are given in Fig. 3), and thus corresponds to the

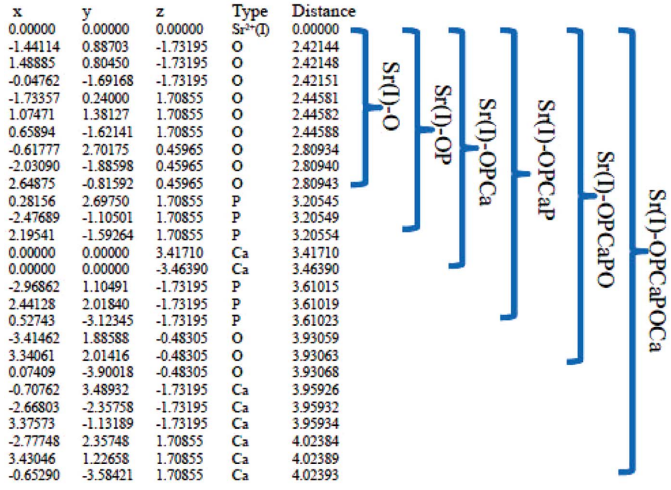

Figure 3
Details regarding the spatial repartition of atoms around Sr^{2+} cations located in site (I).

structural hypothesis. A similar codification has been followed for Sr^{2+} cations in crystallographic site (II). Numerical simulations have been plotted in Figs. 4 and 5.

We must also pay attention to the well known linear variation of the crystallographic parameters with the strontium content. Since the Sr (1.12 Å) ionic radius is larger than that of Ca (0.99 Å), such a substitution process modifies the crystallographic parameters. These structural parameters can be estimated by a linear fit procedure considering the end members $Ca_5(PO_4)_3OH$ (a = 9.432 Å, c = 6.881 Å) and $Sr_5(PO_4)_3OH$ (a = 9.745 Å, c = 7.265 Å) (Kay *et al.*, 1964; Sudarsanan & Young, 1972). These modifications of the cell parameters obviously change the values of the interatomic distances. We have therefore performed a similar set of numerical simulations for different crystallographic parameters (Figs. 6 and 7). With the content of Sr in biological apatite being quite small, we choose the following changes of the cell parameters: a = 9.432 Å and c = 6.881 Å to a = 9.4633 Å and c = 6.9039 Å.

For most of these numerical simulations we observed only a white line at the Sr *K*-edge followed by a simple oscillation of the absorption coefficient as we have observed for experimental data. This is definitely not the case for simulations corresponding to Sr^{2+}(I)-OPCaPO and Sr^{2+}(I)-OPCaPOCa, for which some structures just after the white line have been observed (see arrows in Figs. 4 and 6).

4. Discussion

Concretion, *e.g.* a kidney stone, as well as ectopic calcification often associated with tissue alteration, constitute pathological

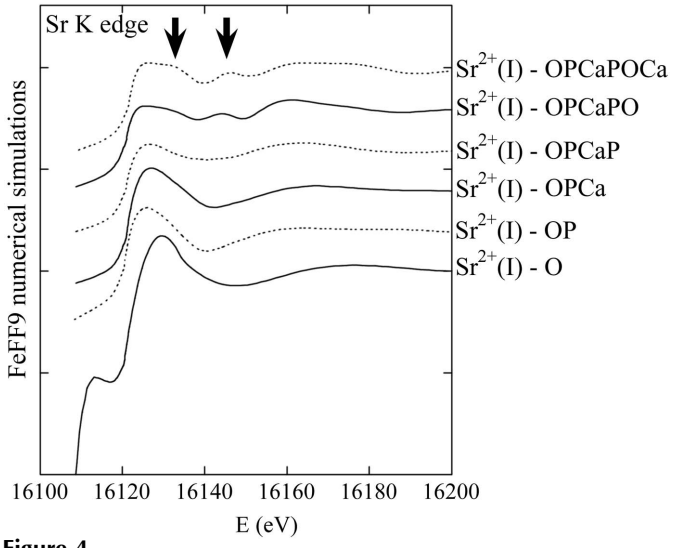

Figure 4
FEFF simulations for the environment of Sr^{2+}(I).

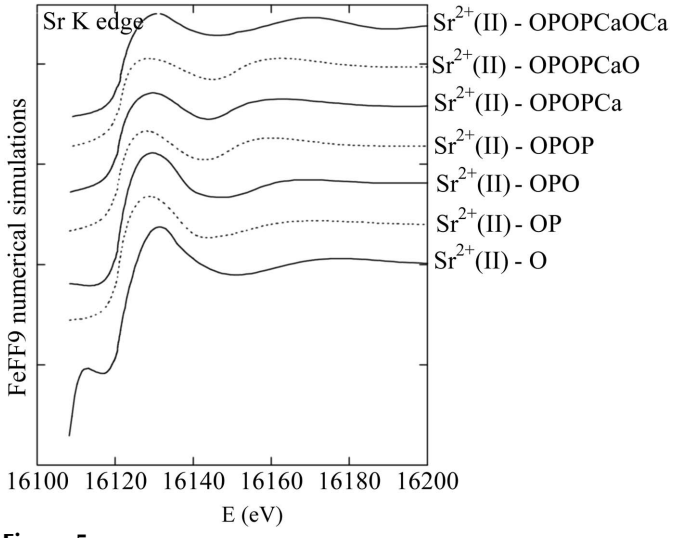

Figure 5
FEFF simulations for the environment of Sr^{2+}(II).

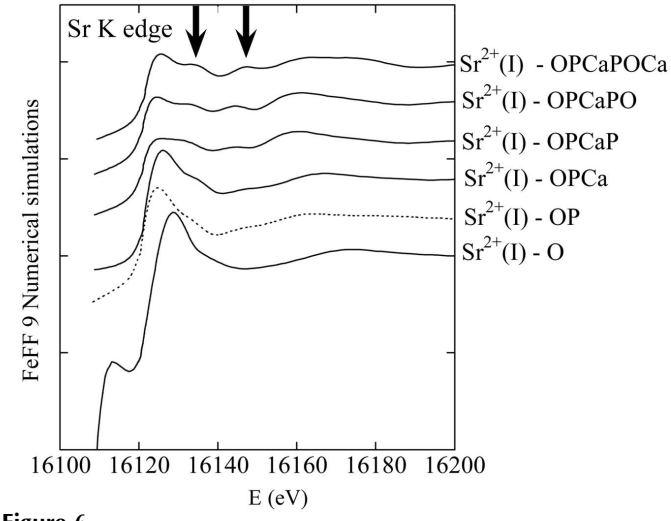

Figure 6
FEFF simulation for the environment of Sr^{2+}(I) (a = 9.4633 Å, c = 6.9039 Å).

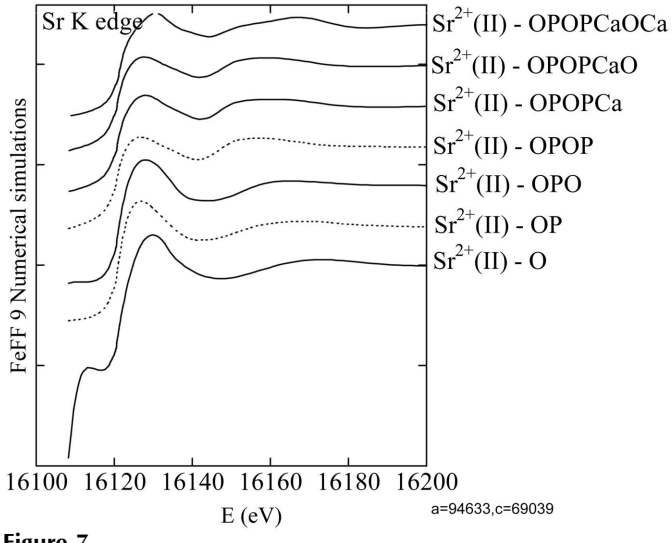

Figure 7
FEFF simulations for the environment of Sr^{2+}(II) (a = 9.4633 Å, c = 6.90039 Å).

calcifications. Also, normal physiological calcifications such as bone or teeth may become pathological through the influence of diseases. Regarding their chemical compositions, numerous chemical phases have been identified. In the case of kidney stones, numerous publications have noted the presence of calcium oxalate, calcium phosphate, uric acid, ammonium hydrogen urate and magnesium ammonium phosphate.

In this study we consider pathological calcifications made of Ca phosphate apatites for which X-ray fluorescence analyses have measured quite a high quantity of strontium equal to 455 $\pm$ 364 $\mu g\ g^{-1}$ (Bazin *et al.*, 2006, 2007). In the case of Ca oxalate the quantity of strontium is quite low ($74 \pm 56\ \mu g\ g^{-1}$). Based on these experimental facts, we can assume that most of the Sr^{2+} cations are linked to the Ca phosphate apatites.

Several publications have discussed the incorporation of Sr^{2+} cations in Ca phosphate apatites, pointing out significant structural modifications for apatite crystals. Among them, a decrease in the dimensions of the coherent length of the perfect crystalline domains at low strontium content was noticed (Bigi *et al.*, 2007; Donnell *et al.*, 2008; Li *et al.*, 2007). An increase of the coherent length is also observed at high strontium content. In contrast, other authors state that the presence of the strontium ion increases the crystallinity as well as crystallite size of HAP (Suganthi *et al.*, 2011). The complete set of such studies indicates that the insertion of Sr^{2+} cations in apatite is a complex process which is sensitive to preparation methods.

Similar structural investigations have been performed on bones and some discrepancy exists among the different results probably due to the experimental protocol, as mentioned for studies on synthetic samples. In an *in vitro* investigation (Korbas *et al.*, 2004), the authors describe a simple Ca^{2+}/Sr^{2+} substitution in the HAP crystal lattice. By contrast, a similar *in vitro* study (Verberckmoes *et al.*, 2004) underlines a potential physicochemical interference by Sr with HAP formation and crystal properties.

Insertion of Sr^{2+} cation in apatites can be discussed from both physiological and chemical points of view. From a physiological point of view, Sr^{2+} cations follow the Ca^{2+} metabolic pathways (Pors Nielsen, 2004). From a chemical point of view, Ca^{2+} and Sr^{2+} have similar chemistry (these two elements sharing the same column in the periodic table), and commonly substitute for one another in minerals (Rokita *et al.*, 1993; Terra *et al.*, 2009).

Regarding Sr^{2+} cation localization in bone, different structural hypotheses take into account the physicochemistry of biological apatites (Fig. 1). At first, Sr^{2+} cations are adsorbed at the surface of collagen or apatite surrounded only by O atoms (hypothesis 1 in Fig. 6). This structural configuration has been studied by Seward *et al.* (1999) through XAS measurements. Sr^{2+} cations can be engaged in the hydrated poorly crystalline apatite part. This structural configuration takes into account the structural model (Cazalbou *et al.*, 2004; Rey *et al.*, 2007) for biological apatites (hypothesis 2 in Fig. 1). Finally, a substitution occurs between Sr^{2+} cations and Ca^{2+} cations inside calcium phosphate nanocrystals either on crystallographic sites (I) or (II) (hypothesis 3 in Fig. 1). In the skeleton the total quantity of Sr is not insignificant, the Sr/Ca being estimated in the human skeleton to be in the range 0.1–0.3 $mg\ g^{-1}$ (Cabrera *et al.*, 1999). This physiological fact offers the opportunity to describe the status of Sr^{2+} cations in biological apatites.

The nature of structural characteristics which can be given by XANES spectroscopy is well known. Such an experimental technique takes advantage of recent theoretical advances which led to the development of several *ab initio* codes for the simulation of X-ray absorption spectra. At the Ca *K*-edge different structural investigations have already used this opportunity (Sowrey *et al.*, 2004; Laurencin *et al.*, 2010).

XANES or EXAFS at the Sr *K*-edge have been used in different materials science studies (Pingitore *et al.*, 1992; Parkman *et al.*, 1998; McKeown *et al.*, 2002; Finch *et al.*, 2003; Singer *et al.*, 2008). In our case we have measured only one oscillation after the Sr *K*-edge in the case of pathological calcifications, while, for physiological calcifications, bones, a clear feature exists just after the white line (Fig. 2).

Regarding numerical simulations, structural hypotheses 1, 2 and 3 have been considered (Fig. 1). Sr^{2+}(I)-O and Sr^{2+}(II)-O correspond to structural hypothesis 1, Sr^{2+}(I)-OP, Sr^{2+}(II)-OP, Sr^{2+}(II)-OPO and Sr^{2+}(II)-OPOP may correspond to hypothesis 2. Finally, Sr^{2+}(I)-OPCa, Sr^{2+}(I)-OPCaO, Sr^{2+}(I)-OPCaOCa, Sr^{2+}(II)-OPOPCa and Sr^{2+}(II)-OPOPCaOCa correspond to hypothesis 3. For the numerical simulations corresponding to structural hypotheses 1 and 2, we observed only a white line at the Sr *K*-edge followed by a simple oscillation of the absorption coefficient as we have observed for experimental data related to pathological calcifications.

At this point we have to emphasize that all Ca phosphates have a high Ca coordination number and low site symmetry. This explains why the role of local lattice distortions has not been taken into account. Since specific XANES features, owing to the first shell, occur with low coordination numbers and high site symmetry, the set of simulations which have been carried out suggest that the additional features are associated with cation–cation scattering enhanced probably by Sr^{2+}–O–(Ca^{2+} or Sr^{2+}) type multiple-scattering paths.

It is worth mentioning that no feature after the white line is observed for Sr^{2+} adsorbed at the surface surrounded only by O atoms and phosphate groups (structural hypotheses 1 and 2). In an opposite way, for simulations corresponding to Sr^{2+} cations inserted in site (I) of HAP [Sr^{2+}(I)-OPCaPO and Sr^{2+}(I)-OPCaPOCa as defined in Fig. 2], some structures exist just after the white line (Figs. 4 and 6). These interesting features show that the localization of Sr^{2+} cations in bones can be assessed through XANES spectroscopy and constitutes an exciting way to complete information coming from other characterization techniques such as scattering ones.

Experimental data seem to indicate that a simple adsorption of Sr^{2+} cations exists in the case of pathological calcifications while an insertion of Sr^{2+} is observed at least for one physiological calcification (BPCart). For the other three physiological samples, AgCart, VECart and VMCart, the evidence is much weaker.

5. Conclusion

Numerous studies have been performed in order to localize the environment of Sr in apatites. The literature shows that the insertion of Sr is quite dependent on the preparation procedure for synthetic as well as *in vitro* samples. In this work biological apatites have been investigated through XANES spectroscopy and a set of numerical simulations using the *FEFF9* program have been performed.

The key point of this structural investigation is related to the opportunity to assess the localization of Sr^{2+} cations in biological apatites through XANES spectroscopy. Owing to the high disorder of the first coordination spheres of Sr, simple adsorption of Sr^{2+} cations at the surface of apatite is related to the absence of features in the XANES part of the X-ray absorption spectra. In contrast, a substitution Sr/Ca with Sr^{2+} cations positioned on crystallographic site (I) gives rise to the presence of features in XANES. The complete set of experimental data seems to indicate that a simple adsorption of Sr^{2+} cations exists in the case of pathological calcifications while an insertion of Sr^{2+} is observed for physiological ones.

Finally, further experiments and numerical simulations taking into account local lattice distortion are called for, to provide definitive evidence of a possible relationship between the nature of the calcification (physiological and pathological) and the adsorption mode of Sr^{2+} cations (simple adsorption or insertion). Is it possible to draw a line between life and chemistry through the localization of Sr in apatite? The question is open for discussion.

This work was supported by the Physics and Chemistry Institutes of CNRS and by a ANR-09-BLAN-0120-02 contract.

References

Ankudinov, A. L., Bouldin, C. E., Rehr, J. J., Sims, J. & Hung, H. (2002). *Phys. Rev. B*, **65**, 104–107.

Ankudinov, A. L., Ravel, B., Rehr, J. J. & Conradson, S. (1998). *Phys. Rev. B*, **58**, 7565–7576.

Bazin, D., Carpentier, X., Brocheriou, I., Dorfmuller, P., Aubert, S., Chappard, C., Thiaudière, D., Reguer, S., Waychunas, G., Jungers, P. & Daudon, M. (2009*b*). *Biochimie*, **91**, 1294–1300.

Bazin, D., Carpentier, X., Traxer, O., Thiaudière, D., Somogyi, A., Reguer, S., Waychunas, G., Jungers, P. & Daudon, M. (2008). *J. Synchrotron Rad.* **15**, 506–509.

Bazin, D., Chappard, Ch., Combes, Ch., Carpentier, X., Rouzière, S., André, G., Matzen, G., Allix, M., Thiaudière, D., Reguer, S., Jungers, P. & Daudon, M. (2009*a*). *Osteoporosis Intl*, **20**, 1065–1075.

Bazin, D., Chevallier, P., Matzen, G., Jungers, P. & Daudon, M. (2007). *Urol. Res.* **35**, 179–184.

Bazin, D., Daudon, M., Chevallier, P., Rouzière, S., Elkaim, E., Thiaudière, D., Fayard, B., Foy, E., Albouy, P. A., André, G., Matzen, G. & Veron, E. (2006). *Ann. Biol. Clin.* **64**, 125–139.

Bazin, D. & Rehr, J. (2003). *J. Phys. Chem. B*, **107**, 12398–12402.

Bazin, D., Sayers, D. & Rehr, J. (1997*a*). *J. Phys. Chem. B*, **101**, 1140–1150.

Bazin, D., Sayers, D., Rehr, J. & Mottet, Ch. (1997*b*). *J. Phys. Chem. B*, **101**, 5332–5336.

Bellis, D. J., Li, D., Chen, Z., Gibson, W. M. & Parsons, P. J. (2009). *J. Anal. At. Spectrom.* **24**, 622–626.

Bigi, A., Boanini, E., Capuccini, C. & Gazzano, M. (2007). *Inorg. Chim. Acta*, **360**, 1009–1016.

Binsted, N., Hasnain, S. S. & Hukins, D. W. (1982). *Biochem. Biophys. Res. Com.* **107**, 89–92.

Boivin, G., Deloffre, P., Perrat, B., Panczer, G., Boudeuille, M., Mauras, Y., Allain, P., Tsouderos, Y. & Meunier, P. J. (1996). *J. Bone Miner. Res.* **11**, 1302–1311.

Bradley, D. A., Moger, C. J. & Winlove, C. P. (2007*b*). *Nucl. Instrum. Methods Phys. Res. A*, **580**, 473–476.

Bradley, D. A., Muthuvelu, P., Ellis, R., Green, E. M., Attenburrow, D., Barrett, R., Arkill, K., Colridge, D. B. & Winlove, C. P. (2007*a*). *Nucl. Instrum. Methods Phys. Res. B*, **263**, 1–6.

Brown, P. W. & Constantz, B. (1994). *Hydroxyapatite and Related Materials.* Boca Raton: CRC Press.

Cabrera, W. E., Schrooten, I., De Broe, M. E. & D'Haese, P. C. (1999). *J. Bone Miner. Res.* **14**, 661–668.

Camacho, N. P., Rinnerthaler, S., Paschalis, E. P., Mendelsohn, R., Boskey, A. L. & Fratzl, P. (1999). *Bone*, **25**, 287–293.

Carpentier, X., Bazin, D., Jungers, P., Reguer, S., Thiaudière, D. & Daudon, M. (2010). *J. Synchrotron Rad.* **17**, 374–379.

Cazalbou, S., Eichert, D., Drouet, Ch., Combes, Ch. & Rey, Ch. (2004). *C. R. Palevol*, **3**, 563–572.

Cooper, C. (1999). *Osteoporosis Intl*, **9**(Suppl. 2), S2–S8.

Dahl, S. G., Allain, P., Marie, P. J., Mauras, Y., Boivin, G., Ammann, P., Tsouderos, Y., Delmas, P. D. & Christiansen, C. (2001). *Bone*, **28**, 446–453.

Daudon, M., Bader, C. A. & Jungers, P. (1993). *Scan. Microsc.* **7**, 1081–1095.

Daudon, M., Bazin, D., André, G., Jungers, P., Cousson, A., Chevallier, P., Véron, E. & Matzen, G. (2009). *J. Appl. Cryst.* **42**, 109–115.

Daudon, M., Junger, P. & Bazin, D. (2008). *N. Engl. J. Med.* **359**, 100–102.

Elliott, J. C. (1994). *Structure and Chemistry of the Apatites and Other Calcium Orthophosphates.* Amsterdam: Elsevier.

Estepa, L. & Daudon, M. (1997). *Biospectroscopy*, **3**, 347–355.

Farlay, D., Boivin, G., Panczer, G., Lalande, A. & Meunier, P. J. (2005). *J. Bone Miner. Res.* **20**, 1569–1578.

Finch, A. A., Allison, N., Sutton, S. R. & Newvilles, M. (2003). *Geochim. Cosmochim. Acta*, **67**, 1189–1194.

Fratzl, P., Schreiber, S., Roschger, P., Lafage, M. H., Rodan, G. & Klaushofer, K. (1996). *J. Bone Miner. Res.* **11**, 248–253.

Gomes, S., Nedelec, J. M., Jallot, E., Sheptyakov, D. & Renaudin, G. (2011). *Chem. Mater.* **23**, 3072–3085.

Grases, F., Genestar, C. & Mill, A. (1989). *J. Cryst. Growth*, **94**, 507–511.

Guinier, A. (1956). *X-ray Diffraction in Crystals, Imperfect Crystals and Amorphous Bodies.* Paris: Dunod.

Harries, J. E., Hukins, D. W. L., Holt, C. & Hasnain, S. S. (1987). *J. Cryst. Growth*, **84**, 563–570.

Holroyd, C., Cooper, C. & Dennison, E. (2008). *Best Pract. Res. Clin. Endocrinol. Metab.* **22**, 671–685.

Hukins, D. W. L., Cox, A. J. & Harries, J. E. (1986). *J. Phys.* C**8**, 1181–1190.

Kay, M. I., Young, R. A. & Posner, A. S. (1964). *Nature (London)*, **204**, 1050–1052.

Korbas, M., Rokita, E., Meyer-Klaucke, W. & Ryczek, J. (2004). *J. Biol. Inorg. Chem.* **9**, 67–76.

Laurencin, D., Wong, A., Chrzanowski, W., Knowles, J. C., Qiu, D., Pickup, D. M., Newport, R. J., Gan, Z., Duer, M. J. & Smith, M. E. (2010). *Phys. Chem. Chem. Phys.* **12**, 1081–1091.

Li, C., Paris, O., Siegel, S., Roschger, P., Paschalis, E. P., Klaushofer, K. & Fratzl, P. (2010). *J. Bone Miner. Res.* **25**, 968–975.

Li, Z. Y., Lam, W. M., Yang, C., Xu, B., Ni, G. X., Abbah, S. A., Cheung, K. M., Luk, K. D. & Lu, W. W. (2007). *Biomaterials*, **28**, 1452–1460.

McKeown, D. A., Kot, W. K. & Pegg, I. L. (2002). *J. Non Cryst. Solids*, **317**, 290–300.

Marie, P. J. (2005). *Curr. Opin. Pharmacol.* **5**, 633–636.
Meunier, P. J., Roux, C., Seeman, E., Ortolani, S., Badurski, J. E., Spector, T. D., Cannata, J., Balogh, A., Lemmel, E. M., Pors-Nielsen, S., Rizzoli, R., Genant, H. K. & Reginster, J. Y. (2004). *N. Engl. J. Med.* **350**, 459–468.
Moonen, J., Slot, J., Lefferts, L., Bazin, D. & Dexpert, H. (1995). *Physica B*, **208–209**, 689–690.
Nguyen, C., Ea, H. K., Thiaudiere, D., Reguer, S., Hannouche, D., Daudon, M., Lioté, F. & Bazin, D. (2011). *J. Synchrotron Rad.* **18**, 475–480.
Ni, G. X., Lu, W. W., Xu, B., Chiu, K. Y., Yang, C., Li, Z. Y., Lam, W. M. & Luk, K. D. K. (2006). *Biomaterials*, **27**, 5127–5133.
O'Donnell, M. D., Fredholm, Y., de Rouffignac, A. & Hill, R. G. (2008). *Acta Biomater.* **4**, 1455–1464.
Oka, T., Yoshioka, T., Koide, T., Takaha, M. & Sonoda, T. (1987). *Urol. Intl*, **42**, 89–93.
Parkman, R. H., Charnock, J. M., Livens, F. R. & Vaughan, D. J. (1998). *Geochim. Cosmochim. Acta*, **62**, 1481–1492.
Paschalis, E. P., Mendelsohn, R. & Boskey, A. L. (2011). *Clin. Orthop. Relat. Res.* **469**, 2170–2178.
Peters, F., Schwarz, K. & Epple, M. (2000). *Thermochim. Acta*, **361**, 131–138.
Pingitore, N. E., Lytle, F. W., DCavies, B. M., Eastmann, M. P., Eller, P. G. & Larson, E. M. (1992). *Geochim. Cosmochim. Acta*, **56**, 1531–1538.
Pors Nielsen, S. (2004). *Bone*, **35**, 583–588.
Rehr, J. J. & Albers, R. C. (2000). *Rev. Mod. Phys.* **72**, 621–660.
Rehr, J. J., Kas, J. J., Prange, M. P., Sorini, A. P., Takimoto, Y. & Vila, F. (2009). *C. R. Phys.* **10**, 548–559.
Rey, Ch., Combes, Ch., Drouet, C., Lebugle, A., Sfihi, H. & Barroug, A. (2007). *Materialwiss. Werkst. Tech.* **38**, 996–1002.
Rochefort, G. Y., Pallu, S. & Benhamou, C. L. (2010). *Osteoporosis Intl*, **21**, 1457–1469.
Rokita, E., Hermes, C., Nolting, H. F. & Ryczek, J. (1993). *J. Cryst. Growth*, **130**, 543–552.
Roschger, P., Manjubala, I., Zoeger, N., Meirer, F., Simon, R., Li, C., Fratzl-Zelman, N., Misof, B. M., Paschalis, E. P., Streli, C., Fratzl, P. & Klaushofer, K. (2010). *J. Bone Miner. Res.* **25**, 891–900.
Roux, Ch. (2007). *Bone*, **40**, S9–S11.
Sayers, D. A., Stern, E. A. & Lytle, F. W. (1971). *Phys. Rev. Lett.* **27**, 1204–1207.
Seward, T. M., Henderson, C. M. B., Charnock, J. M. & Driesner, T. (1999). *Geochim. Cosmochim. Acta*, **63**, 2409–2418.
Singer, D. M., Johnson, S. B., Catalano, J. G., Farges, F. & Brown, G. E. (2008). *Geochim. Cosmochim. Acta*, **72**, 5055–5069.
Sowrey, F. E., Skipper, L. J., Pickup, D. M., Drake, K. O., Lin, Z., Smith, M. E. & Newport, R. J. (2004). *Phys. Chem. Chem. Phys.* **6**, 188–192.
Sudarsanan, K. & Young, R. A. (1972). *Acta Cryst.* B**28**, 3668–3670.
Suganthi, R. V., Elayaraja, K., Ahymah Joshy, M. I., Sarah Chandra, V., Girija, E. K. & Narayana Kalkura, S. (2011). *Mater. Sci. Eng.* **31**, 593–601.
Tamm, T. & Peld, M. (2006). *J. Solid State Chem.* **179**, 1581–1587.
Terra, J., Dourado, E. R., Eon, J. G., Ellis, D. E., Gonzalez, G. & Rossi, A. M. (2009). *Phys. Chem. Chem. Phys.* **11**, 568–577.
Verberckmoes, S. C., Behets, G. J., Oste, L., Bervoets, A. R., Lamberts, L. V., Drakopoulos, M., Somogyi, A., Cool, P., Dorriné, W., De Broe, M. E. & D'Haese, P. C. (2004). *Calcif. Tissue Intl*, **75**, 405–415.
White, T. J. & ZhiLi, D. (2003). *Acta Cryst.* B**59**, 1–16.
Wilson, R. M. & Elliott, J. C. (1999). *Am. Mineral.* **84**, 1406–1414.
Zhang, Y., Cheng, F., Li, D., Wang, Y., Zhang, G., Liao, W., Tang, T., Huang, Y. & He, W. (2005). *Biol. Trace Elem. Res.* **103**, 177–185.
Zheng, Y., Jin, W., Wanga, C., Yang, M., Shen, H., Eisa, M. H. & Mi, Y. (2009). *Nucl. Instrum. Methods Phys. Res. B*, **267**, 2128–2131.
Zoeger, N., Streli, C., Wobrauschek, P., Jokubonis, C., Pepponi, G., Roschger, P., Hofstaetter, J., Berzlanovich, A., Wegrzynek, D., Chinea-Cano, E., Markowicz, A., Simon, R. & Falkenberg, G. (2008). *X-ray Spectrom.* **37**, 3–11.